Biosensors and Bioelectronics 170 (2020) 112547

Contents lists available at ScienceDirect

Biosensors and Bioelectronics

journal homepage: http://www.elsevier.com/locate/bios

Optical fiber bio-sensor for phospholipase using liquid crystal

Jieyuan Tang [a,b,1], Zhibin Li [a,b,1], Mengyuan Xie [a,b], Yu Zhang [b], Wenjin Long [b], Shun Long [c], Tianjin Wen [b], Zhanxiong Fang [b], Wenguo Zhu [a,b], Huadan Zheng [a,b], Yunhan Luo [a,b], Heyuan Guan [a,b], Huihui Lu [a,b], Jun Zhang [a,b], Jianhui Yu [a,b,*], Zhe Chen [a,b,**]

[a] Key Laboratory of Optoelectronic Information and Sensing Technologies of Guangdong Higher Education Institutes, Jinan University, Guangzhou, 510632, China
[b] Department of Optoelectronic Engineering, Jinan University, Guangzhou, 510632, China
[c] Department of Computer Science, Jinan University, Guangzhou, 510632, China

ARTICLE INFO

Keywords:
Biosensor
Fiber
Side-polished fiber
Liquid crystal
Phospholipase A2

ABSTRACT

A cost-effective and label-free optical fiber sensor was proposed to detect phospholipase A_2 (PLA_2) in nM concentration. The sensor is made of an alkoxysilane-modified side-polished fiber (SPF) coated with 4′-pentyl-4-cyanobiphenyl (5CB) and self-assembled phospholipid (L-DLPC). It is found that the relative transmission optical power (RTOP) of the fiber sensor decreases due to the 5CB realignment and redistribution induced by the PLA_2 hydrolysis of L-DLPC. The response-time at 5 dB RTOP variation exhibits an exponential dependence on PLA_2 concentration, allowing us to detect the PLA_2 by the 5 dB-response time. This detection method can reduce the detection time. Compare with the traditional copper-grid sensor, the proposed novel fiber sensor has a lower detection limit (<1 nM). Furthermore, the sensor has good repeat-ability and specificity.The sensor's RTOP variation for PLA_2 detection at 1 nM is ~21 times higher than that for five other enzymes (trypsin, amylase, thrombin, glucose oxidase, pepsin) at 1000 nM and lipase at 50 nM. This confirms the sensor's excellent PLA_2 specificity. The fiber sensor provides a potential way to be incorporated into micro-flow chips to quantitatively detect biological molecules in a real-time and online manner.

1. Introduction

Phospholipases play an important role in various biochemical processes (Waite, 1987). They are usually divided into several categories, among which phospholipase A_2 (PLA_2) is a good marker for some diseases (Kalyvas and David, 2004; Sun et al., 2004), especially cardiovascular diseases (Niessen et al., 2003). Therefore, the detection of PLA_2 is of great significance for medical diagnosis. The state-of-the-art methods for PLA_2 detection include fluorescence analysis (Abe et al., 2018; Li et al., 2016), electrochemical method (Jablonowska et al., 2011) and magnetic resonance (Cheng and Tsourkas, 2014). Complex chemical preprocesses are usually necessary in electrochemical method. Fluorescence analysis and magnetic resonance require labeling bio-molecules and expensive equipment. By now, there is a desirable but challenging demand for a simple and convenient detection method.

Liquid Crystals (LCs) are sensitive materials in sensing field (Song et al., 2019; Wang et al., 2018a). In 1998, Abbott group first proposed the use of thermotropic LC film for biochemical sensing (Gupta et al., 1998), which arises a boom of research on LC-based biochemical sensors (Shah and Abbott, 2001; Bi and Yang, 2008; Bai and Abbott, 2012; Lai et al., 2011). In 2003, Abbott group sandwiched the LC-filled grid cell between a slide and the aqueous solution (Brake et al., 2003), the biochemical molecules in aqueous solution can be observed with naked-eye (Zhong and Jang, 2014; Wang et al., 2015; Chuang et al., 2016). Recently, this detection system has been further simplified by dropping the LC droplets directly in aqueous solution (Wang et al., 2018b; Munir and Park, 2018; Deng et al., 2018). In addition, some other systems have also been proposed, including microcapillary confined LCs (An and Jang, 2018; Kim and Jang, 2017) and LC/polymer fiber mats (Wang et al., 2018c). LC-based sensors have attracted great interest of researchers (Luan et al., 2020; Popov et al., 2018). However, it cannot work without conventional polarizing optical microscope (POM).

Optical fiber sensor offers a promising alternative platform to

* Corresponding author. Department of Optoelectronic Engineering, Jinan University, Guangzhou, 510632, China.
** Corresponding author. Department of Optoelectronic Engineering, Jinan University, Guangzhou, 510632, China.
E-mail addresses: jianhuiyu@jnu.edu.cn (J. Yu), thzhechen@jnu.edu.cn (Z. Chen).
[1] Co-first author: Jieyuan Tang and Zhibin Li.

https://doi.org/10.1016/j.bios.2020.112547
Received 6 February 2020; Received in revised form 19 August 2020; Accepted 22 August 2020
Available online 25 August 2020

implement biological sensor due to its advantages (Montserrat and Manuel, 2012). Recently, various optical fiber structures have been reported for biochemical sensors (Arcas et al., 2018; Cao et al., 2018; Zhou et al., 2019; Kumar et al., 2019). Among these fiber structures, the side-polished fiber (SPF) has significant advantages in easy fabrication and low cost, and its D-shape cross section makes feasible a flat platform onto which various kinds of sensitive material can be easily integrated (Jang et al., 2009; Wen et al., 2015; Yu et al., 2014).

In this paper, we propose a novel sensor based on a SPF onto which LC and phospholipid are integrated. The hydrolysis of phospholipid by PLA_2 triggers the realignment and redistribution of LC on the sensor, which not only alters the effective refractive index of LC but also induces the change of the transmission light power of the fiber sensor. Our designed fiber sensor avoids the use of bulky, expensive POM, and achieves real-time, on-line and quantitative measurement of biochemical molecules.

2. Material and methods

2.1. Materials

Tris base, L-a-dilauroyl phosphati-dylcholine (L-DLPC), 4′-pentyl-4-cyanobiphenyl (5CB), dimethyloctadecyl[3-(trimethoxysilyl)propyl] ammonium chloride (DMOAP) and trypsin (≥10,000 BAEE units/mg) were purchased from Sigma-Aldrich. Thrombin (2000 units/mg), pepsin (>3000 units/mg) and amylase (4000 units/g) were purchased from Shanghai Makclin Biochemical Co., Ltd. Phospholipase A_2 (PLA_2, from Eastern Diamondback rattlesnake venom, ≥200 units/mg) was purchased from Shanghai Aladdin Biochemical Technology Co., Ltd. Lipase (≥1000 units/mg) and glucose oxidase (100–250 units/mg) were purchased from Guangzhou Dingguo Biotechnology Co., Ltd. Hydrogen peroxide, concentrated sulfuric acid, sodium chloride, calcium chloride, hydrochloric acid, sodium hydroxide and ethanol were purchased from Guangzhou Chemical Reagent Factory. Deionized water was purchased from Guangzhou Haosheng Biotechnology Co. Ltd.

2.2. Fabrication of SPF

The SPF was fabricated with standard single-mode fiber (SMF, Corning SMF-28e+) by wheel-based side-polished technique (Tang et al., 2017). The core and cladding are all made of silica. The diameter of core is ~9 μm and the cladding is ~125 μm. Fig. 1(a) shows the schematic of SPF structure. The inset in the left-bottom of Fig. 1(a) shows the microscopic image of the cross section of the fabricated SPF in our experiment. The residual thickness of the flat region is ~66.41 μm. The length of the polished section is ~8 mm, while that of the flat region is ~5 mm (Fig. 1(b)).

2.3. Modification of SPF with DMOAP

The fabricated bare SPF was firstly hydroxylated by immersing it into "piranha solution" (70% H_2SO_4 and 30% H_2O_2) for 30 min at room temperature (Fig. 2(a)). Then, the treated SPF was rinsed with plenty of deionized water. Next, the SPF was modified with dimethyloctadecyl [3-(trimethoxysilyl)propyl] ammonium chloride (DMOAP) by being immersed into 0.5% DMOAP aqueous solution for 10 min at room temperature (Fig. 2(b)). Finally, the immersed SPF was rinsed with plenty of deionized water again and heated in 120°C for 1h (Fig. 2(c)).

2.4. Overlay of LC onto the SPF

The DMOAP modified SPF was fixed on a clean glass slide with the polished surface facing up (Fig. 2(d)). After heated up to 40°C, the LC (5CB) was smeared on the surface of the DMOAP-modified SPF (Fig. 2 (e)). The left-bottom inset of Fig. 2(e) shows the POM image of the LC-coated SPF, which is schematically shown in the right-bottom inset of Fig. 2(e).

2.5. Modification of the LC-coated SPF with phospholipid

In the modification, the LC-coated SPF with DMOAP was firstly immersed into TBS solution (10 mM Tris, 100 mM NaCl, pH8.9). Then,

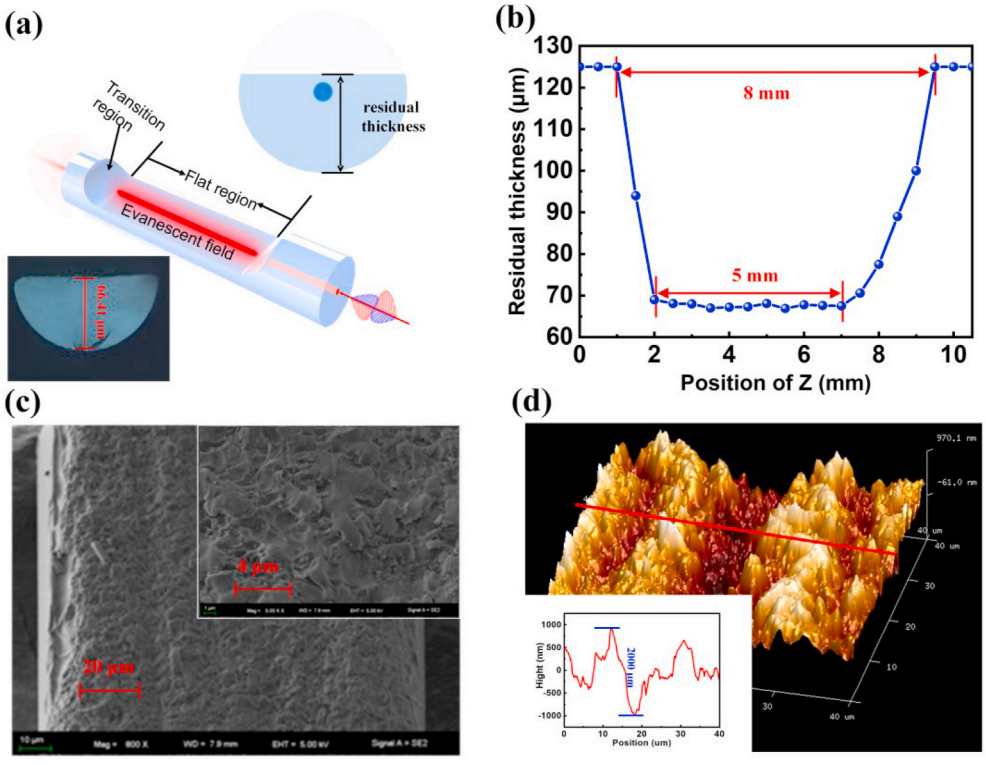

Fig. 1. (a) Schematic of a bare SPF structure; the inset at the bottom-left is the microscopic image of the SPF′ cross section. (b) Residual thickness variation along the SPF. (c) Scanning electron microscopic and (d) atomic force microscopic images of the polished surface of the SPF. The inset in (c) is the local enlarged view. The inset in (d) shows the height variation across the red line. (For interpretation of the references to colour in this figure legend, the reader is referred to the Web version of this article.)

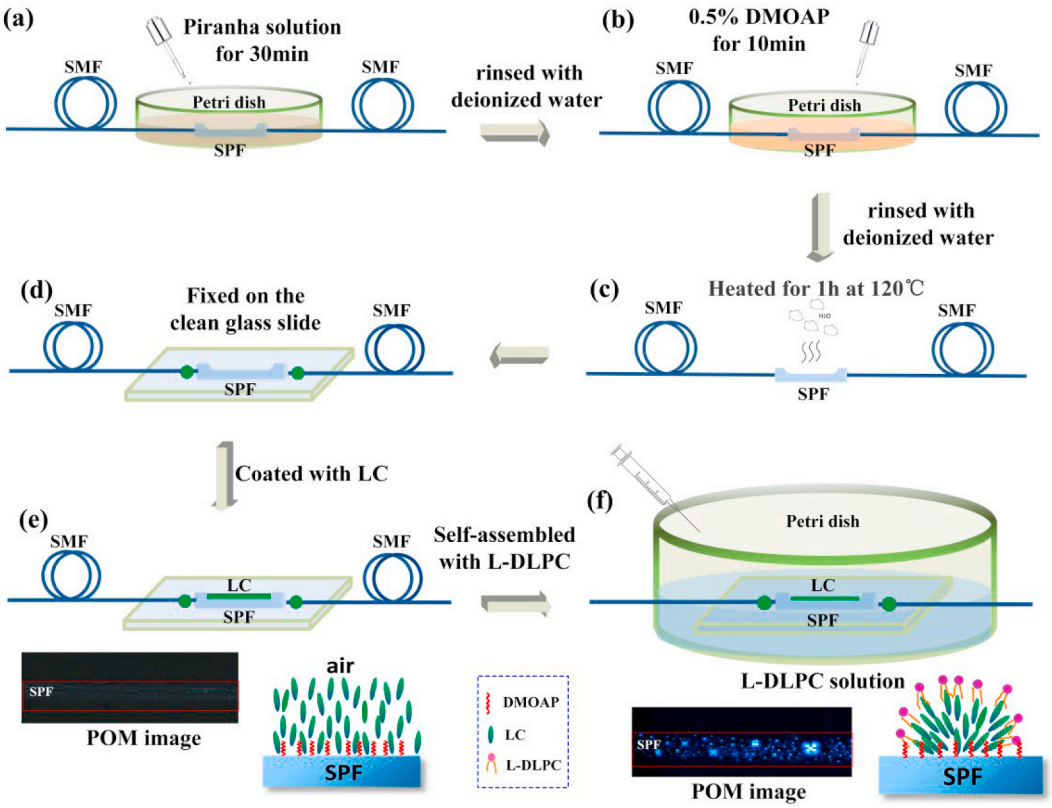

Fig. 2. Steps of the fabrication of the fiber sensor. (a) The hydroxylation of the fabricated SPF in Piranha solution; (b) modifying the polished surface of SPF with DMOAP; (c) heating the DMOAP-modified SPF; (d) fixing the SPF on a clean glass slide; (e) coating LC on the SPF. The left-bottom inset is the POM image; the right-bottom inset shows the schematic of aligning LC by DMOAP on the SPF; (f) self-assembling L-DLPC at the aqueous/LC interface on the SPF. The left-bottom inset shows the POM image and the right-bottom inset shows L-DLPC realigns and deforms LC.

phospholipid (L-DLPC) solution was injected (Fig. 2(f)). L-DLPC gradually self-assembled at the aqueous/LC interface, which accordingly realigns and redistributes the LC, as seen in the left-bottom inset of Fig. 2 (f). Finally, the excessive L-DLPC in the solution was flushed out completely.

2.6. Experimental setup and sensing principle

Fig. 3(a) shows the experimental setup for the LC-coated fiber sensor for PLA_2 detection. The fiber sensor was placed in a petri dish and the LC on the fiber sensor was continuously monitored with a POM. A light beam launched from a DFB laser (1310 nm, SOFII-A, Accelink Technologies Co., Ltd) was coupled into a polarization controller. The light beam passes through the LC-coated region of the fiber sensor. Finally, the power variation was measured and recorded by the optical power meter (6210, Shanghai Guangwei Communications Co., Ltd). All the experiments were carried out at an ambient temperature of 25 °C and a relative humidity of 67.5%. Before the experiments, the output power of the DFB laser was monitored for 10 h (Fig. S1 in Supplementary). The fluctuation of the DFB laser was measured as ±0.02 dB, indicating the laser is stable enough for accurate detection.

Fig. 3(b) illustrates the principle of PLA_2 detection for the fiber sensor. Before PLA_2 detection, the fiber sensor is modified with the PLA_2-recognition molecules (L-DLPC), the L-DLPC molecules self-assemble at the aqueous/LC interface of the sensor. The L-DLPC self-assembly makes the LC deforms into semicircular droplets, as shown in the left of Fig. 3(b) (Brake and Abbott, 2002). When PLA_2 is detected, the L-DLPC will be hydrolyzed into 1-lauroyl-2-hydroxy-sn-glycero-3--phosphocholine and free fatty acid, and then desorbed from the aqueous/LC interface (Hartono et al., 2008; Brake et al., 2003) of the sensor. This hydrolysis process causes the LC droplets to collapse into films as shown in the right of Fig. 3(b), increasing the leakage of the transmitted light from the polished-surface of the sensor. Whereby, the hydrolysis of L-DLPC by PLA_2 can be detected by the transmission power of the fiber sensor.

3. Results and discussion

3.1. Characteristics of the SPF

Before fabricating the SPFs, we computed the electric field distribution of the SPF with different residual thickness. As the residual thickness deceases from 67.5 μm to 63.5 μm, the electric field intensity near the polished surface becomes stronger (Fig. S2 in Supplementary). However, in our experiments, the smaller the residual thickness is, the greater the SPF's insertion loss becomes. So, the residual thickness of the fabricated SPF is optimally chosen as ~66.5 μm and the insertion loss is measured as 7–8 dB in the air.

Fig. 1(c) shows the SEM images of the SPF's polished surface. The polished surface is rough and contains several grooves, which is further verified by AFM as shown in Fig. 1(d). The depth of the grooves is ~2 μm. The grooves play an important role in stabilizing LC on the SPF. Variation in the transmission optical power of the SPF with the ambient refractive index (ARI) was measured and is shown in Fig. S3 in Supplementary. The transmission optical power drops sharply with the ARI in the range of 1.44–1.46, while rises in the ARI range of 1.46–1.65. This relation provides an essential mechanism to detect optical refractive index change in the LC caused by the PLA_2 hydrolysis.

3.2. Characteristics of the LC-coated SPF

Fig. 4(a) shows the relative transmission optical power (RTOP)

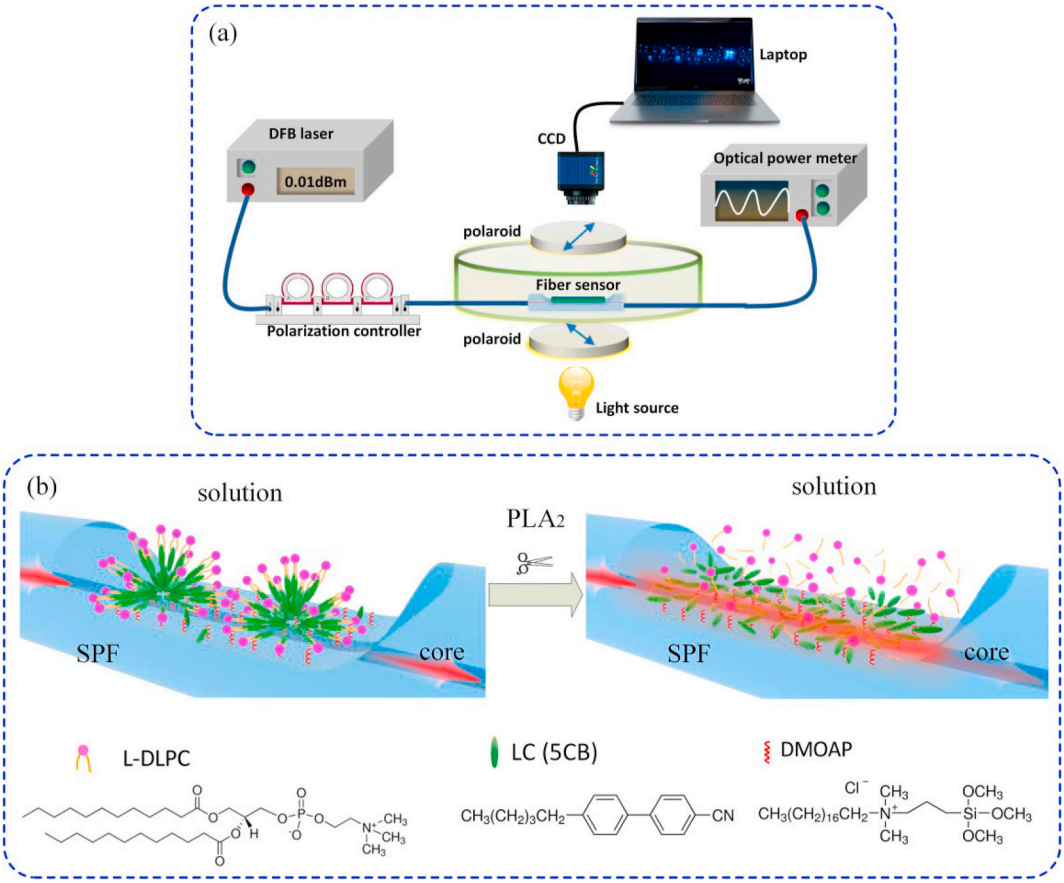

Fig. 3. (a) Experimental setup; (b) principle of the fiber sensor for PLA_2 detection.

variation of the DMOAP-modified SPF in the air, the average power is about -0.12 dB and the maximum fluctuation is ±0.12 dB for 12 min. When the SPF is coated with LC, the RTOP of the SPF decreases from -0.12 dB to -19.25 dB (Fig. 4(a) and (b)). The large attenuation of optical power is due to the fact that the effective refractive index of the LC coated on the SPF is larger than that of the SPF core, which destroys the total reflection condition of the SPF. As shown in the inset of Fig. 2(e), the dark POM image indicates that the LC coated on the SPF is homeotropic aligned. Fig. 4(c) shows the TROP variation of the LC-coated SPF when the SPF is immersed into TBS solution for estimation of the aqueous solution impact to the LC realignment on the SPF. The RTOP of the SPF changes dramatically and disorderly for about 6 min (see the green shaded section of Fig. 4(c)). This is because the immersion of the LC-coated SPF in TBS solution is disturbing the LC alignment. Then, the RTOP starts to increase and tends to stabilize at -31.2 dB (the yellow shaded section of Fig. 4(c)). This is because the LC on the SPF completes the homeotropic-to-planar realignment at the aqueous/LC interface and a hybrid alignment of the LC film is formed (the inset of Fig. 4(c)). The LC realignment changes the effective refractive index of LC and induces the RTOP variation.

To further clarify the DMOAP effectiveness, another LC-coated SPF was fabricated with the same parameters, but without DMOAP modification. Fig. 4(d) shows the RTOP variation of the LC-coated SPF without DMOAP in TBS solution. The RTOP rises rapidly from -21.1 dB to -10.5 dB in 3 s at the moment of being immersed into TBS solution (the inset of Fig. 4(d)), and finally stabilizes at -4.5 dB, almost identical to the RTOP of the bare SPF without LC in TBS solution. It indicates that the LC coated on the SPF without DMOAP is almost washed away. This confirms that the DMOAP not only triggers the homeotropic alignment of the LC at the LC/SPF interface, but also prevents the LC from being washed away in TBS solution and promotes the stability of LC coated on the SPF.

3.3. Characteristics of the SPF modified with phospholipid

Phospholipid (L-DLPC) works as the specific recognition molecule for the proposed fiber sensor. Fig. 5(a) and (b) present the RTOP variation of the LC-coated SPF, respectively, in 0.33 mM and 0.1 mM L-DLPC solution. When L-DLPC molecules gradually self-assemble at the aqueous/LC interface (the inset of Fig. 5(a)), the RTOP of the SPF drops quickly from -29.5 dB to -39.1 dB in the first ~5 min (the green shaded section of Fig. 5(a)) and then starts to rise exponentially from -39.1 dB to 0.5 dB in the next ~90 min (the yellow shaded section of Fig. 5(a)). The RTOP changes can be up to 30 dB, indicating that the LC-coated SPF is ultrasensitive to the L-DLPC self-assembly. To give insight into the sensing mechanism, the RTOP variation and the morphologic image of the LC-coated SPF were, respectively, monitored by optical power meter and POM, as shown in Fig. 5(b). The RTOP variation in Fig. 5(b) behaves in a similar way to that in Fig. 5(a), but the response-time in Fig. 5(b) increases threefold whilst the L-DLPC concentration decreases threefold. This indicates that higher concentration of L-DLPC could accelerate the L-DLPC self-assembly speed at the solution/LC interface. From the POM images in the insets of Fig. 5(b), it can be seen that the polished surface of the LC-coated SPF appears bright initially because of the LC hybrid alignment. Then, the SPF gradually gets dark as L-DLPC self-assembling at the LC/aqueous interface. About 0.5 h later, the bright fan-like spots appear on the SPF. Finally, the bright spots get smaller and smaller in the next 4 h and the RTOP turns unchanged. The microscopic insets indicate that the hybrid aligned LC on the SPF converges into semicircular droplets and turns polar alignment under the impact of L-DLPC self-assembly.

The RTOP variation of the LC-coated SPF induced by the L-DLPC self-

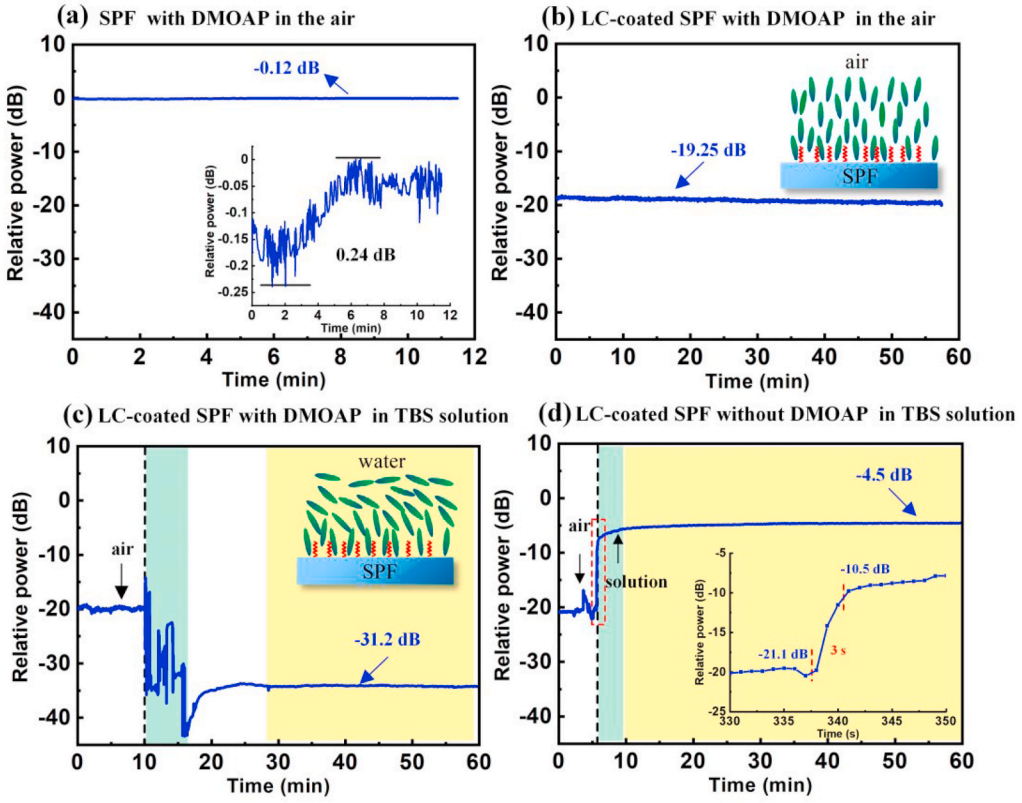

Fig. 4. The RTOP variation of the DMOAP-modified SPF (a) in the air, (b) coated with LC in the air, and (c) coated with LC in TBS solution. (d) The RTOP variation of the bare SPF coated with LC in TBS solution.

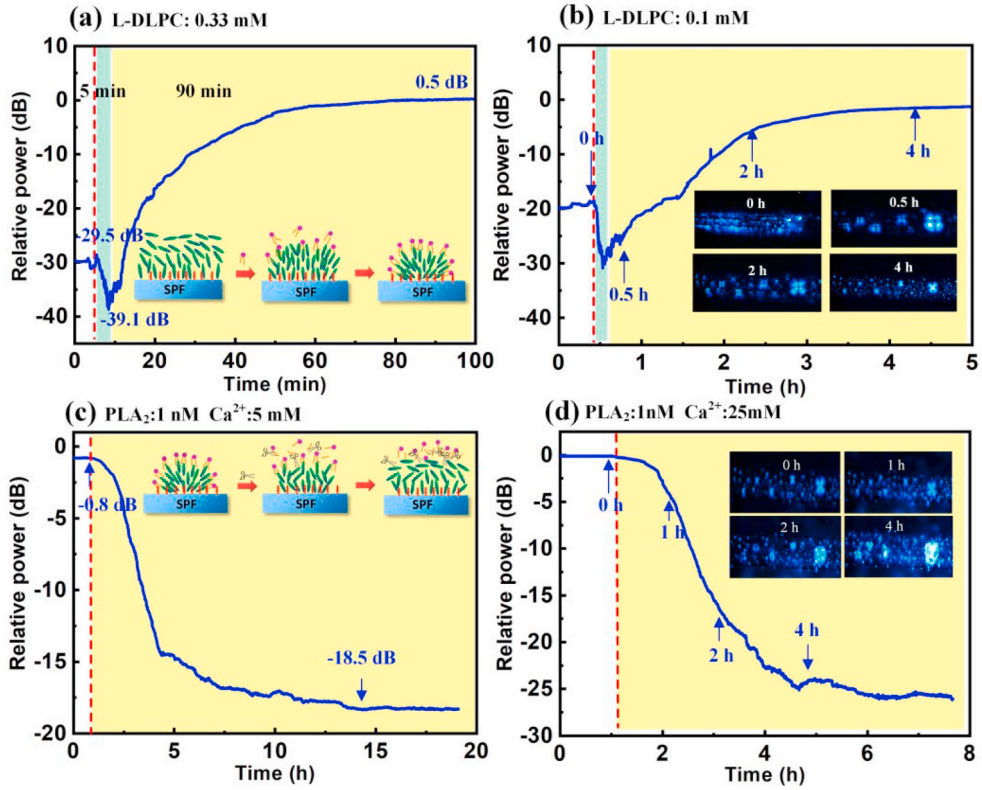

Fig. 5. Variation in the RTOP of the LC-coated SPF immersed into L-DLPC solution of (a) 0.33 mM or (b) 0.1 mM. The inset in (a) is schematic of the L-DLPC self-assembly on the LC. The insets in (b) are POM images of the LC-coated SPF. The RTOP of the sensor in 1 nM PLA_2 at the present of (c) 5 mM or (d) 25 mM Ca^{2+}. The inset in (c) is the schematic of the L-DLPC hydrolysis process by PLA_2. The insets in (d) are POM images of the sensor in 1 nM PLA_2, 25 mM Ca^{2+}.

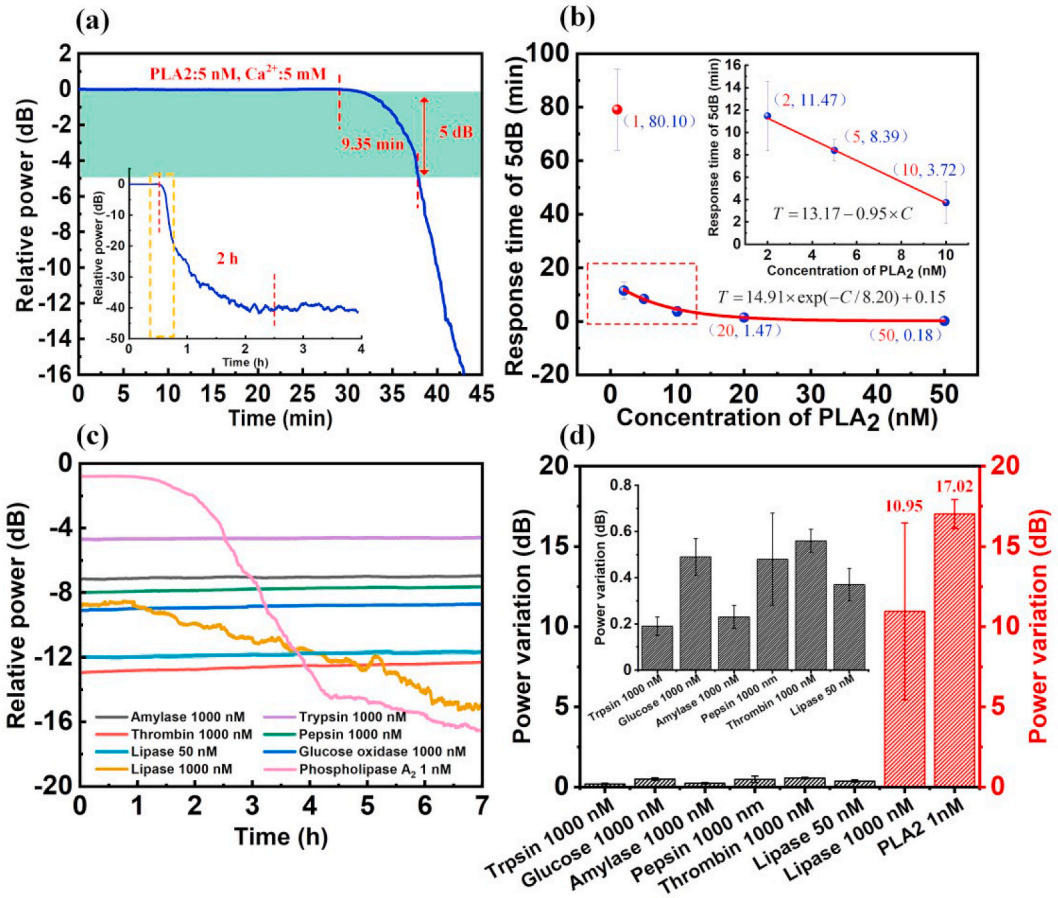

Fig. 6. (a) The RTOP variation of the sensor in 5 nM PLA_2, 5 mM Ca^{2+} solution, which is the local enlarged view in the yellow dotted box of the inset. (b) The response-time at 5 dB change RTOP on the different PLA_2 concentration. The inset in (b) is the local enlarged view of the red dotted box. (c) The RTOP of the fiber sensor to the different enzyme. (d) The RTOP variation of the fiber sensor for different enzyme in 7 h. The inset in (d) is the local enlarged view of (d). (For interpretation of the references to colour in this figure legend, the reader is referred to the Web version of this article.)

assembly can be explained by the change in effective refractive index of the LC on the SPF. Before the L-DLPC self-assembly, LC is hybrid alignment as shown in the first inset of Fig. 5(a), and the effective refractive index of LC could be estimated as $(n_e + n_o)/2$ (~1.58) (Han et al., 2014). The LC on the SPF turns into homeotropic alignment and deforms into semicircular droplets during the L-DLPC self-assembly, which decreases the LC's effective refractive index. As a result, according to the relation between the RTOP of the bare SPF and the ARI as presented in Fig. S3 in Supplementary, the RTOP of the LC-coated SPF should be theoretically expected to fall at the beginning and then arise as shown in Fig. 5(a) and (b). It is seen that the above theoretical explanation is in good consistency with the experiments.

3.4. Detection of phospholipase A_2 (PLA_2)

When the LC-coated SPF was immersed into the L-DLPC solution and L-DLPC self-assembly at the LC/aqueous interface finished, the fiber sensor completed its fabrication process and had specifically sensitivity to PLA_2. The excess L-DLPC in the solution was flushed away to avoid the influence on PLA_2 concentration detection. Fig. 5(c) shows the response of the sensor to PLA_2. The RTOP of the sensor decreases from -0.8 dB to -18.5 dB in 1 nM PLA_2, 5 mM Ca^{2+} solution. PLA_2 is a kind of calcium dependent enzyme, and calcium ions play a key role in the hydrolysis process of L-DLPC. Without Ca^{2+}, the sensor would fail to respond. Fig. 5 (c) and (d) show that an increase of the Ca^{2+} concentration from 5 mM to 25 mM can significantly speed up the PLA_2 response. This confirms that Ca^{2+} can promote the hydrolysis process of L-DLPC. The corresponding dynamic POM images in the insets of Fig. 5(d) reveal that the semicircular LC droplets change during the L-DLPC hydrolysis by PLA_2. Initially, there are bright fan-like spots on the plat surface of the fiber sensor. After 1 h, there appear more and more small fan-like spots. Roughly ~2 h later, the fan-like spots turn into bright spots and grow bigger and bigger. After 4 h, the fan-like spots completely disappear, instead, more big and bright spots appear. This series of changes of bright spots reveals that the LC droplets are collapsed by the L-DLPC hydrolysis with PLA_2 and deform into several lamellar films with the LC hybrid alignment as shown in the schematic insets of Fig. 5(c). As a result, the L-DLPC hydrolysis with PLA_2 leads to an increase in the effective refractive index of the LC and thus decreases the sensor RTOP, as theoretically expected as shown in Fig. S3.

Fig. S4 demonstrates the response of the sensor to various concentrations of PLA_2 in the presence of 5 mM Ca^{2+}. The response-time is ~14 h when the power of the sensor turns stable for 1 nM PLA_2. For 10 nM, it is ~1.5 h. If the PLA_2 concentration increases to 50 nM, the response-time goes down to ~11 min. The results suggest that the concentration of PLA_2 can be estimated by the response-time of the sensor. However, the response-time of the sensor is too long for low PLA_2 concentration. It is more than ten hours for ~1 nM PLA_2, which is unacceptable for the detection of biological enzymes in practice. To accelerate the detection process, we propose the response-time at 5 dB change RTOP (Fig. 6(a)) as the sensing parameter for the PLA_2 concentration detection. The detection-time of the sensor decreases from ~2 h to ~9 min for 5 nM PLA_2. This reduction in the detection-time indicates the method is very suitable for low concentration bio-

molecule. Fig. 6(b) shows the relation between the 5 dB-response-time T and PLA_2 concentration C. It is fitted well to the exponential function.

$$T = 14.91 \times \exp(-C/8.20) + 0.15 \quad (1)$$

with a high correlation coefficient of 0.9955. We also find that in the concentration range of 2–10 nM, as seen in the inset of Fig. 6(b), experimental results fit well to the following function:

$$T = 13.17 - 0.95 \times C \quad (2)$$

The high linear coefficient of 0.9983 indicates the good linearity of the sensor in the range.

As shown in Fig. S4, the RTOP of the sensor decreases as 17.5 dB for 1 nM PLA_2 in 14 h. If the concentration decreases to 0.1 nM, the RTOP variation of the sensor is only 0.9 dB in 10 h. Thus, the detection limit of the sensor to PLA_2 can inferred to be in the range of 0.1 nM–1 nM. Fig. S5 demonstrates three RTOP variations of the sensor for three repeated experiments at 1 nM PLA_2. Three almost identical RTOP variations indicates the sensor has good repeat-ability. The average 5 dB-response-time for 1 nM PLA_2 is 80.1 min and relative standard deviations (RSD) is 14.4%.

To assess the specificity of the fiber sensor, the fiber sensor was used to detect seven different kinds of enzyme. The RTOPs of the fiber sensors for the seven enzymes are shown in Fig. 6(c). The results show that the fiber sensor is insensitive to trypsin, pepsin, glucese oxidase, thrombin, amylase with a RTOP variation of less than 0.8 dB in 7 h at 1000 nM, as seen in the inset of Fig. 6(d). However, RTOP decreased by 10.95 dB in 7 h for 1000 nM lipase, indicating that the sensor is also sensitive to lipase which is a hydrolytic enzyme that acts on carboxylic ester bonds. Nevertheless, if the lipase goes down to 50 nM, the RTOP variation of the sensor is less than 0.6 dB in 7 h. In the concentration range of 0–50 nM, the RTOP variation of the fiber sensor for the PLA_2 is at least 21 times higher than that for other enzymes, indicating the fiber sensor has pretty good specificity to PLA_2.

To compare the traditional copper-grid sensor (CGS) with the proposed fiber sensor, we have carried the PLA_2 detection experiment by the copper-grid method (See Supplementary). Fig. S6 shows the POM image variation of the CGS in different PLA_2 concentrations. As shown in Fig. S6, the L-DLPC-induced hydrolysis (Hartono et al., 2008; Brake et al., 2003) makes the LC in the copper-grid realign, and thus gradually increases the brightness of POM image for the CGS under the PLA_2 concentration higher than 2 nM. The brightness is, here, extracted and spatially averaged from the bright pattern in the copper-grid, and its time-dependence is shown in Fig. S7(a) for the various PLA_2 concentrations. The stable brightness B exhibits an exponential relation with the PLA_2 concentration C as shown in Fig. S7(b), which can be fitted well to

$$B = -0.95 \times \exp(-C/8.26) + 0.91 \quad (3)$$

with a high correlation coefficient of 0.9911. Additionally, it can be seen in Fig. S7(a) that the CGS detection limit is around 2 nM, which is higher than the 1 nM detection limit of the proposed fiber sensor. This is because the proposed fiber sensor has longer sensitive region than the CGS through which the light passes, and thus higher sensitivity than the CGS.

Here, we also propose the response-time at 5 dB change RTOP of the fiber sensor as the sensing parameter to reduce the detection time. With the help of the calibration curve proposed above (Fig. 6(b)), the fiber sensor can quantitatively detect PLA_2 in real-time by using 5 dB-respond-time. However, as shown in Fig. S7, the brightness of the CGS can detect the PLA_2 concentration until the brightness become stable. In addition, unlike the CGS method, the proposed fiber sensor has the advantages of compact-size, low-cost, in-line detection, which is suitable to be incorporated into a micro-flow chip for quick biochemical detection.

4. Conclusions

A simple and label-free biochemical fiber sensor based on the LC optical amplification and its characteristics were demonstrated. The exponential relationship between the response-time at a 5 dB RTOP variation of the fiber sensor and PLA_2 concentration allows us to drop the detection time of 1 nM concentration to ~80 min. Additionally, the RTOP variation to PLA_2 is at least 21 times higher than that to other six enzymes, suggesting that the fiber sensor has a pretty good specificity. The detection limit of the proposed LC-coated fiber sensor can be low as 1 nM, which is lower than the CGS of ~2 nM. Although the proposed fiber sensor is only demonstrated for the PLA_2 detection ex vivo, the fiber senor can be generalized to other biochemical molecules using other kind of recognition molecule. Furthermore, the configuration of the proposed fiber sensor provides a potential way to be incorporated into a micro-flow chip for faster quantitative detection of biochemical molecules in real-time and on-line.

Declaration of competing interest

The authors declare that they have no known competing financial interests or personal relationships that could have appeared to influence the work reported in this paper.

Acknowledgement

This work was supported by National Natural Science Foundation of China (61675092, 61705086, 61601404), Natural Science Foundation of Guangdong Province (2020B1515020024, 2017A030313375), Special Funds for Major Science and Technology Projects of Guangdong Province (2019B010138004, 2017A010102006), Project of Guangzhou Industry Leading Talents (CXLJTD-201607), Joint Fund of Pre-research for Equipment, Ministry of Education of China (6141A02022124), Foundation for Distinguished Young Talents in Higher Education of Guangdong (2018KQNCX009), Fundamental Research Funds for the Central Universities (11617333).

Appendix A. Supplementary data

Supplementary data to this article can be found online at https://doi.org/10.1016/j.bios.2020.112547.

References

Abe, A., Hiraoka, M., Shayman, J.A., Ohguro, H., 2018. Anal. Biochem. 549, 164–170.
An, Z.F., Jang, C.H., 2018. Sensor. Actuator. B Chem. 269, 135–142.
Arcas, A.D., Dutra, F.D., Allil, R.C.S.B., Werneck, M.M., 2018. Sensors 18, 648.
Bai, Y.Q., Abbott, N.L., 2012. J. Am. Chem. Soc. 134, 548–558.
Bi, X.Y., Yang, K.L., 2008. Sensor. Actuator. B Chem. 134, 432–437.
Brake, J.M., Abbott, N.L., 2002. Langmuir 18, 6101–6109.
Brake, J.M., Daschner, M.K., Luk, Y.Y., Abbott, N.L., 2003. Science 302, 2094–2097.
Cao, S.Q., Shao, Y., Wang, Y., Wu, T.S., Zhang, L.F., Huang, Y.J., Zhang, F., Liao, C.G., He, J., Wang, Y.P., 2018. Op. Express 26, 3988-2994.
Cheng, Z.L., Tsourkas, A., 2014. Sci. Rep. 4, 6958.
Chuang, C.H., Lin, Y.C., Chen, W.L., Chen, Y.H., Chen, Y.X., Chen, C.M., Shiu, H.W., Chang, L.Y., Chen, C.H., Chen, C.H., 2016. Biosens. Bioelectron. 78, 213–220.
Deng, J.N., Wang, X.C., Liang, W.L., Richardson, D., Lu, Q., Fanga, J.Y., 2018. Colloids Surf. A Physicochem. Eng. Asp. 542, 52–58.
Gupta, V.K., Skaife, J.J., Dubrovsky, T.B., Abbott, N.L., 1998. Science 279, 2077–2080.
Han, Y.Q., Chen, Z., Cao, D., Yu, J.H., Li, H.Z., He, X.L., Zhang, J., Luo, Y.H., Lua, H.H., Tang, J.Y., Huang, H.K., 2014. Sensor. Actuator. B Chem. 196, 663–669.
Hartono, D., Bi, X.Y., Yang, K.L., Yung, L.Y.L., 2008. Adv. Funct. Mater. 18, 2938–2945.
Jablonowska, E., Wieckowska, A., Rogalska, E., Bilewicz, R., 2011. J. Electroanal. Chem. 660, 360–366.
Jang, H.S., Park, K.N., Kim, J.P., Sim, S.J., Kwon, O.J., Han, Y.G., Lee, K.S., 2009. Opt. Expr. 17, 3855–3860.
Kalyvas, A., David, S., 2004. Neuron 41, 323–335.
Kim, H.J., Jang, C.H., 2017. Chem. Phys. Lipids 204, 10–14.
Kumar, S., Kaushik, B.K., Singh, R., Chen, N.K., Yang, Q.S., Zhang, X., Wang, W.J., Zhang, B.Y., 2019. Biomed. Opt. Express 10, 2150–5160.
Lai, S.L., Tan, W.L., Yang, K.L., 2011. ACS Appl. Mater. Interfaces 3, 3389–3395.

Li, J.L., Zhang, Y.H., Ai, J.J., Gao, Q., Qi, H.L., Zhang, C.X., Cheng, Z.L., 2016. RSC Adv. 6, 15895–15899.
Luan, C.L., Luan, H.P., Luo, D.W., 2020. Micromachines 11, 176.
Montserrat, F.V., Manuel, L.A., 2012. Sensors 12, 3929–3951.
Munir, S., Park, S.Y., 2018. Sensor. Actuator. B Chem. 257, 579–585.
Niessen, H.W.M., Krijnen, P.A.J., Visser, C.A., Meijer, C.J.L.M., Hack, C.E., 2003. Cardiovasc. Res. 60, 68–77.
Popov, N., Honaker, L.W., Popova, M., Usol'tseva, N., Mann, E.K., Jakli, A., Popov, P., 2018. Materials 11, 20.
Shah, R.R., Abbott, N.L., 2001. Science 293, 1296–1299.
Song, B.Y., Hu, J.Y., Xia, C.L., Zhang, H., Lu, Y.L., Sun, W.M., Liu, Y.J., 2019. Appl. Optic. 58, 410–414.
Sun, G.Y., Xu, J.F., Jensen, M.D., Simonyi, A., 2004. J. Lipid Res. 45, 205–213.
Tang, J.Y., Zhou, J.J., Guan, J.W., Long, S., Yu, J.H., Guan, H.Y., Lu, H.H., Luo, Y.H., Zhang, J., Chen, Z., 2017. IEEE J. Sel. Top. Quant. 23, 5600708.
Waite, M., 1987. The Phospholipases. Plenum, New York.
Wang, Y., Hu, Q.Z., Guo, Y.X., Yu, L., 2015. Biosens. Bioelectron. 72, 25–30.
Wang, J.R., Jakli, A., West, J.L., 2018c. J. Mol. Liq. 267, 490–495.
Wang, F.R., Liu, Y.J., Lu, Y.L., Zhang, L.L., Ma, J., Wang, L., Sun, W.M., 2018a. Opt. Lett. 43, 5355–5358.
Wang, Y., Zhao, L.Y., Xu, A.J., Wang, L., Zhang, L.L., Liu, S.Q., Liu, Y.J., Li, H.Y., 2018b. Sensor. Actuator. B Chem. 258, 1090–1098.
Wen, S.C., Chang, C.W., Lin, C.M., Hsiao, V.K.S., Yu, J.H., Chen, Z., 2015. Optic Commun. 334, 110–114.
Yu, J.H., Han, Y.Q., Huang, H.K., Li, H.Z., Hsiao, V.K.S., Liu, W.P., Tang, J.Y., Lu, H.H., Zhang, J., Luo, Y.H., Zhong, Y.C., Zang, Z.G., Chen, Z., 2014. Opt. Expr. 22, 5950–5961.
Zhong, S.H., Jang, C.H., 2014. Biosens. Bioelectron. 59, 293–299.
Zhou, L., Liu, C., Sun, Z.B., Mao, H.J., Zhang, L., Yu, X.F., Zhao, J.L., Chen, X.F., 2019. Biosens. Bioelectron. 137, 140–147.